Journal of ELECTRONIC MATERIALS, Vol. 48, No. 5, 2019
https://doi.org/10.1007/s11664-018-06917-6
© 2019 The Minerals, Metals & Materials Society

CrossMark

Effect of Rare Earth Metals on the Properties of Zn-20Sn High-Temperature Lead-Free Solder

JUN TIAN,[1,2,3] CHUNFU HONG,[2,3] LIHUA HONG,[2,3] XIAOHUI YAN,[2,3] and PINQIANG DAI[1,2,3,4]

1.—School of Materials Science and Engineering, Fuzhou University, Fuzhou, China. 2.—School of Materials Science and Engineering, Fujian University of Technology, Fuzhou, China. 3.—Fujian Provincial Key Laboratory of Advanced Materials Processing and Application, Fuzhou, China. 4.—e-mail: pqdai@126.com

Cerium–lanthanum mixed rare earth (RE) (0.5 wt.%) was added to Zn-20Sn high-temperature lead-free solder to study the effect of RE on the solder properties. The Zn-20Sn-0.5RE solder has a better corrosion resistance than that of Zn-20Sn alloy. RE addition increases the γ-Cu_5Zn_8 layer thickness, promotes growth of a ε-$CuZn_5$ layer shaped like bamboo shoots, and increases the roughness of the ε-$CuZn_5$ layer, which increases the shear strength of the solder joints. Compared with the Zn-20Sn alloy, the creep resistance of the Zn-20Sn-0.5RE solder was improved after soldering. The indentation hardness increases in an order of Zn-20Sn-0.5RE solder, Zn-20Sn solder, ε-$CuZn_5$ layer, and γ-Cu_5Zn_8 layer.

Key words: Zn-20Sn alloy, high-temperature lead-free solder, corrosion resistance, interfacial reaction, shear strength, nano-indentation

INTRODUCTION

High-lead solders, such as 95Pb-5Sn and 90Pb-10Sn, have been applied commonly in high-temperature electronic packaging. However, lead is toxic to human beings, and its application is restricted globally. Because a suitable alternative material has not been found, high-lead solders are allowed in some cases. Thus, the development of a new high-temperature lead-free solder that can replace traditional high-lead solder and other lead-free interconnect processes has become an urgent requirement in electronics packaging.[1]

Zn-Sn-based solder does not generate intermetallic compounds (IMCs) and has advantages of an appropriate melting temperature range, better plasticity, better thermal/electrical conductivity and low cost, so it is an alloy that is most likely to replace high-lead solders.[2–5] To solve the problems of the poor wettability and poor oxidation resistance of the Zn-Sn-based solder, an alloying method may be used to improve its properties.[6] When a small amount of rare earth (RE) is added, the surface tension of Sn-Ag-Cu solder may be reduced during soldering, which promotes solder wetting on the substrate.[7] In addition, it is found that the solder wettability could be improved by the addition of 0.5 wt.% cerium–lanthanum mixed RE in Zn-20Sn.[8] However, the effect of RE on the performance of solder joints made of Zn-20Sn alloy has not been reported. In present paper, the mechanical behavior, microstructure, wettability, and corrosion resistance of solder joints of Zn-20Sn and Zn-20Sn-0.5RE solders were investigated, and the effect of the RE on the IMC layer at solder/Cu interface was investigated. The results provide a reference for the development of new high-temperature lead-free solders.

EXPERIMENTAL PROCEDURES

RE elements (0.5 wt.%) were added to Zn-20Sn alloy. Zn particles and Sn particles with a purity of more than 99.9 wt.% were selected. The weight

(Received July 16, 2018; accepted December 29, 2018; published online January 8, 2019)

ratio of Ce and La was 65/35 in the mixed RE blocks. The mass fraction of Ce and La exceeded 99% in the total mass of REs. The alloys were prepared by the method as described in the literature.[8]

A wettability test was conducted at five different temperatures (400°C, 410°C, 420°C, 430°C, and 440°C) using a wetting balance (RHESCA 5200TN, made in Japan). A copper sheet (30 mm × 5 mm × 0.3 mm) was soaked in absolute ethanol and washed ultrasonically for 5 min. The copper sheet was dipped into molten solder with an immersion rate of 5 mm/s. After being dipped to a depth of 3 mm for 5 s, then the copper sheet was lifted up with rate of 5 mm/s. The wetting time is given on the JIS Z 3198.

Polarization curves for the solder alloy were measured by using an electrochemical tester (Autolab 302). Sodium-chloride aqueous solution (5%) was used as a corrosive medium. The reference electrode was a saturated calomel electrode and the auxiliary electrode was a platinum electrode. The test temperature was 20°C. The potential scanning range was − 0.1 V to 0.1 V. The scanning rate was 0.001 V/s.

The Cu substrate used for shear strength test was 50 mm × 10 mm × 1 mm and the lap area was 10 mm × 5 mm. After the Cu substrate was polished, it was soaked in 10% hydrochloric acid solution for 10 s, washed with absolute ethanol, and blown dry. Solder pieces (10 mm × 5 mm × 0.15 mm) were coated with flux, placed between two Cu substrates, and then heated in furnace at 440°C for 300 s. As contrast, the Pb-5Sn alloy is heated at 350°C for 300 s.

The pieces were removed with air-cooling. The loading speed of the electronic universal testing machine was 1 mm/min. The shear fracture area was measured by using an Auto CAD. The data for each sample were an average of three samples.

After spreading test, which was conducted at soldering temperature of 440°C with soldering time of 300 s, the spreading specimen was cut down in center. Half of the sample was used for microstructure observation by using cold inlay processing and mechanical polishing. For the other half of the sample, solder surface was polished first until it was close to the Cu substrate. Then, it was placed in 10 vol.% hydrochloric acid/alcohol solution, and deep etching was performed on the solder to expose the interfacial IMC. The interface microstructure was observed by using Hitachi S-3400 N scanning electron microscopy (SEM). Compositional analysis was performed by using a QUANTAX EDS and the interfacial IMC thickness was measured.

Thickness of the interfacial IMCs was measured for each layer. Thickness of the ε-$CuZn_5$ was calculated by using a software. Its thickness was measured and calculated according to:

$$H = \frac{A}{L} \tag{1}$$

where H is the thickness of the IMC layer, A is the area of the IMC layer, and L is the length of the IMC layer for the selected region. According to the literature,[9] the roughness was calculated as:

$$R_{\mathrm{rms}} = \sqrt{\frac{1}{N}\sum_{i=1}^{N} Z_i^2} \tag{2}$$

where R_{rms} is the roughness (μm), N is the number of measurement points in the selected area, and Z_i is the distance from IMC peak value of the measurement area to the measurement baseline (μm). The thickness of ten points of the center area at the interface was measured. Then, the IMC roughness at the interface was obtained by the measurement and calculation.

Indentation hardness and creep properties of the solders were measured by using a TI-Premier nanoindenter. The constant applied load was 6 mN. The applied load rate was 100 μN/s. The duration time was 120 s. The unloading time was 60 s.

EXPERIMENTAL RESULTS AND DISCUSSION

Wettability

The wettability time of the Zn-20Sn-0.5RE and Zn-20Sn solder alloys on Cu substrate at various soldering temperature is shown in Fig. 1.

It can be seen that the wetting time of the Zn-20Sn-0.5RE alloy on the Cu sheet decreased gradually with an increase of soldering temperature. The wetting time was the shortest at 440°C and the solder wettability was the best. When the soldering temperature was 400°C, the wetting time increased by the addition of 0.5% RE and the wetting effect was poor. The addition of RE has almost no effect on the wetting time at temperature of 410–440°C.

The wetting time was strongly dependent on the interface reaction occurred between the solder and substrate.[10] It could be inferred from the wetting

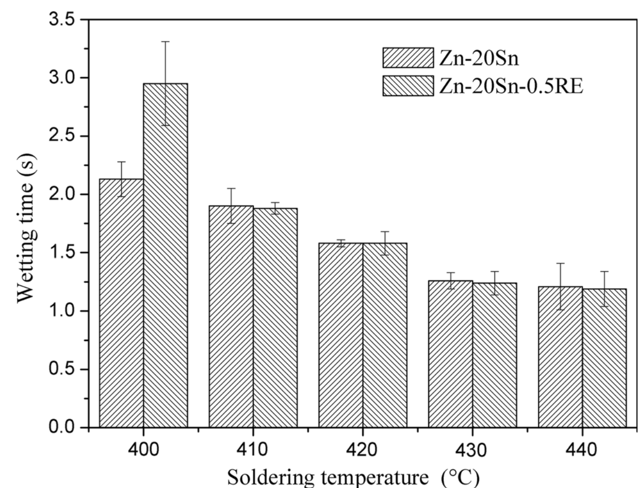

Fig. 1. Relationship between soldering temperature and wettability time.

time that the reaction rate increased with an increase in soldering temperature. In order to obtain a better wettability, the soldering temperature should exceed 430°C.

Electrochemical Corrosion

Polarization curves of the Zn-20Sn and Zn-20Sn-0.5RE in 5% NaCl solution are shown in Fig. 2. The corrosion voltage and corrosion current density are obtained by the curve fitting, as shown in Table I.

In Table I, Zn-20Sn-0.5RE alloy has a smaller corrosion current density and higher corrosion voltage. It shows the electrochemical corrosion resistance property of Zn-20Sn-0.5RE alloy is better than that of Zn-20Sn alloy. In addition, previous work indicates that adding small amount of RE (Ce, Er and Y) into Zn-5Al alloy can obviously improve the corrosion resistance of the alloy. This behaviour may be ascribed to improved protective properties of the corrosion products layer, which acts as an effective barrier against corrosion progress.[11] As REs may improve protective properties of the corrosion products layer, thus enhances the corrosion resistance of the Zn-20Sn alloy.

Interfacial IMC

Microstructures of the solder joint at a soldering temperature of 440°C and a soldering time of 300 s are shown in Fig. 3. The Zn-Sn binary phase diagram shows that the microstructure of Zn-20Sn solder consists of primary α-Zn and eutectic structure (α-Zn + β-Sn), as shown in Fig. 3a. The dissolution speed of the Cu substrate into liquid solder is rapid and it diffuses rapidly deep into the liquid phase, which result in the formation of interfacial IMC layer. With reference to the research on the interfacial reaction between Zn-Sn solder and the Cu substrate,[2–5] the IMC layer at the interface consists of three parts: the bamboo-shoot-like ε-$CuZn_5$ near the solder side, the flat-layer-like β'-CuZn near the Cu side, and the flat-layer-like γ-Cu_5Zn_8 in the middle. The β'-CuZn layer thickness is very thin and is usually less than 1 μm, which is often ignored in the literature.[2] As confirmed by EDS, ε-$CuZn_5$ of dendritic growth may be isolated existing in the solder. Actually, the isolated ε-$CuZn_5$ was some cross-section of the bamboo-shoot-like ε-$CuZn_5$ that grows from the interface as shown in Fig. 3b.

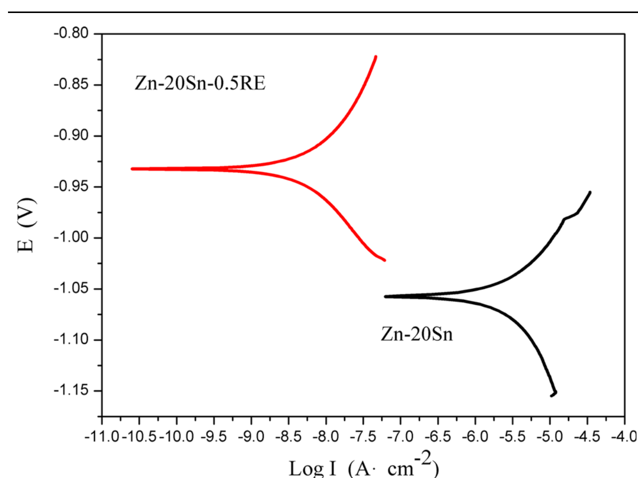

Fig. 2. Polarization curves of solder alloys.

Table I. Electrochemical corrosion data of solder alloys

Solder	Corrosion voltage (V)	Corrosion current density (μA/cm^2)
Zn-20Sn	− 1.051	2.904
Zn-20Sn-0.5RE	− 0.941	0.006

After adding 0.5 wt.% RE, the compound containing REs is shown in Fig. 3c. XRD fails to detect this compound because of its low content. RE addition promotes the growth of the ε-$CuZn_5$ and γ-Cu_5Zn_8 layer at the interface, especially the bamboo-shoot-like growth of ε-$CuZn_5$, as shown in Fig. 3d.

Figure 3d shows that the bamboo-shoot-like growth of the ε-$CuZn_5$ of the IMC layer at the solder interface with 0.5 wt.% RE addition in the alloy is more intense, that is, Cu diffused deeply into the solder. The interfacial roughness of the ε-$CuZn_5$ layer of Zn-20Sn alloy is 1.44, and the interfacial roughness of the ε-$CuZn_5$ layer of the Zn-20Sn-0.5RE alloy is 7.09. After 0.5 wt.% RE addition, the γ-Cu_5Zn_8 layer thickness of the IMC increases by 12.4%, whereas the thickness of the ε-$CuZn_5$ layer of the IMC increases by 30%. The roughness of the ε-$CuZn_5$ layer is increased by 392.4%.

Research results on middle-temperature solders show that when the wetting of liquid Sn-based solder and Cu substrate occurred, the following relationship of force equilibrium must be satisfied at the grain boundary during IMC grain growth at the interface between the solder and Cu.[9,12] In the present work, the equilibrium of the force at the grain boundary of $CuZn_5$ is studied.

$$\gamma_{gb} = 2\gamma_{il}\cos\theta_{il} \tag{3}$$

where γ_{gb} is the grain boundary energy of the $CuZn_5$, γ_{il} is the interfacial energy between the $CuZn_5$ grains and liquid solder at the interface, and θ_{il} is the equilibrium half-angle of the $CuZn_5$ grains at the interface.

A schematic diagram of the force-equilibrium condition at grain boundary in liquid-phase reaction is shown in Fig. 4.

The value of the equilibrium half-angle θ_{il} at grain boundaries of the $CuZn_5$ depends mainly on the interfacial energy, γ_{il} between the $CuZn_5$ grain and liquid solder. γ_{il} is affected by the solder

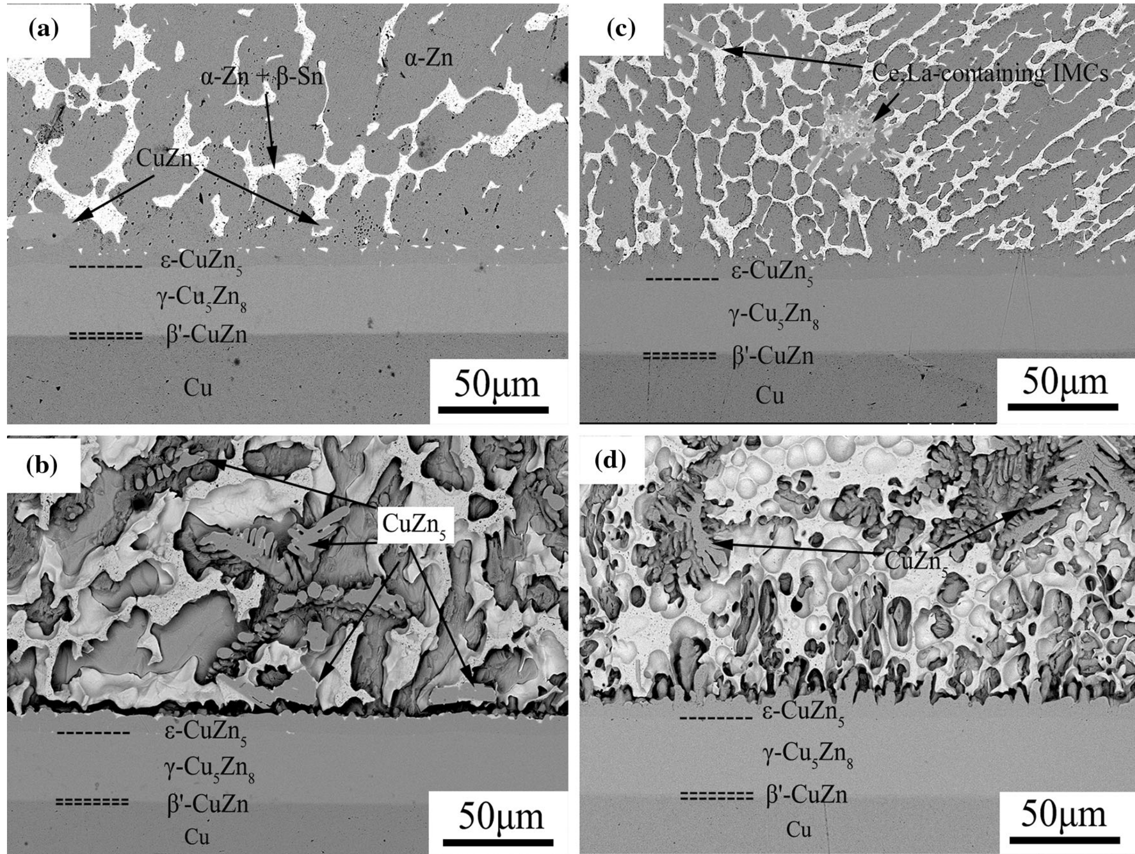

Fig. 3. Cross-sectional SEM micrographs of the interface between solder alloys and Cu substrate: (a) Zn-20Sn, (c) Zn-20Sn-0.5RE, SEM micrographs of the interface between solder alloys and Cu substrate after etching. (b) Zn-20Sn, (d) Zn-20Sn-0.5RE.

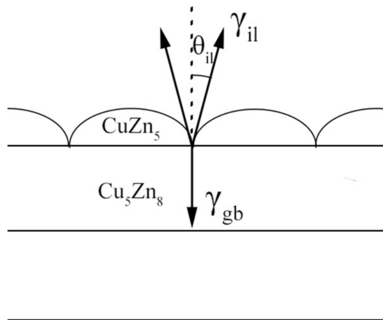

Fig. 4. Schematic diagram of force-equilibrium condition at grain boundary in liquid-phase reaction.

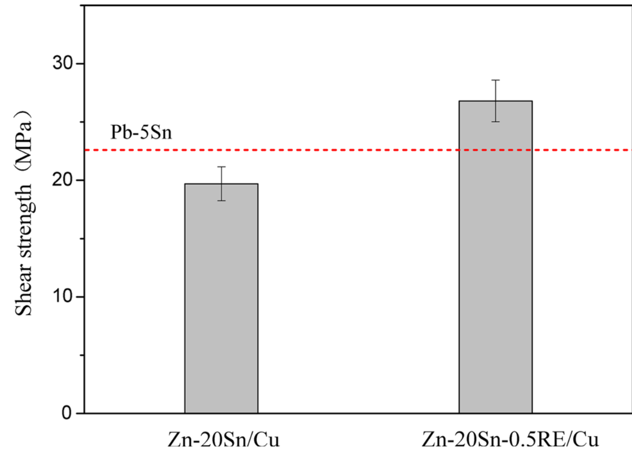

Fig. 5. Shear strength of soldered joints.

composition and reaction temperature.[9] In this study, the reaction temperature was the same, whereas the solder composition was different. After RE addition, the bamboo-shoot-like growth of the ε-$CuZn_5$ was strong and the equilibrium half-angle decreased. Thus, the interfacial energy of the γ_{il} between the ε-$CuZn_5$ grains and liquid solder decreased. RE addition resulted in a decreased interfacial energy between the solid and liquid, which resulted in a strong growth of bamboo-shoot-like ε-$CuZn_5$.

Earlier, it was indicated that the increase in IMC roughness at the interface of the Sn-Pb solder/Cu leads to a decrease in crack resistance with high-speed propagation after the solder joints have been heated for a long time, which is not conducive to the wetting and spreading of solder on the substrate.[13]

In this study, a similar results are obtained. That is the IMC roughness of solder/Cu interface has no influence on the spreading area of the test solders, even the IMC roughness of Zn-20Sn-0.5RE/Cu interface is larger than that of Zn-20Sn.

Shear Strength

The effect of 0.5 wt.% RE addition on the shear strength of soldered joints is shown in Fig. 5. The shear strength of the solder joint of the Zn-20Sn solder alloy is about 20 MPa, which is lower than that of the solder joint of the Pb-5Sn solder alloy (23.1 MPa). However, the shear strength (26.8 MPa) of the Zn-20Sn-0.5RE solder joint is higher than that of the Pb-5Sn, and the solder joint exhibit an excellent mechanical property.

It may be mentioned that the shear strength of Zn-20Sn/Cu joint is lower than that given in the literature (about 31–33 MPa).[14] This is related to the heating temperature and holding time during soldering. In order to obtain better wettability, the soldering joint was heated at 440°C for 300 s. The shear strength of Zn-20Sn/Cu was lower because of the thickening of IMC layer at the interface.

The thickness and morphology of IMC at the interface correlate well with the strength of the solder joint. After RE addition, thickness of the γ-Cu_5Zn_8 and ε-$CuZn_5$ layer was increased. The IMC roughness at the interface increased. The ε-$CuZn_5$ with a bamboo-shoot-like structure is embedded into the solder like numerous nails, which improves the bonding strength of the solder and substrate.[15] However, if the flat γ-Cu_5Zn_8 layer is too thick at the interface, the shear strength of the soldered joints may decrease because of its high brittleness.

Micromechanical Behavior of Interface

The nano-indentation technique has been used extensively to characterize the mechanical properties of the local area and creep properties of solder joints.[16–18] Two layers of IMCs of ε-$CuZn_5$ and γ-Cu_5Zn_8 formed between the solder alloy and the Cu substrate. Using the nano-indentation test, the indentation hardness of the IMC and solders are obtained. Load–displacement curves of each phase at the interface and the solder alloys are shown in Fig. 6.

Figure 6 shows that the γ-Cu_5Zn_8 is the hardest phase in the interfaces. With the predetermined load of 6 mN, the maximum indentation depth of the γ-Cu_5Zn_8 phase is the shallowest in all the phases, followed by ε-$CuZn_5$. The solder hardness is smaller. The hardness of the Zn-20Sn-0.5RE solder is lower than that of the Zn-20Sn solder. Figure 6 shows that the displacement increases nonlinearly with loading. For 120 s with a maximum load of 6 mN, platforms with different lengths appear in various curves. During this process, the displacement deepens with time. At this time, creep occurs in each phase.

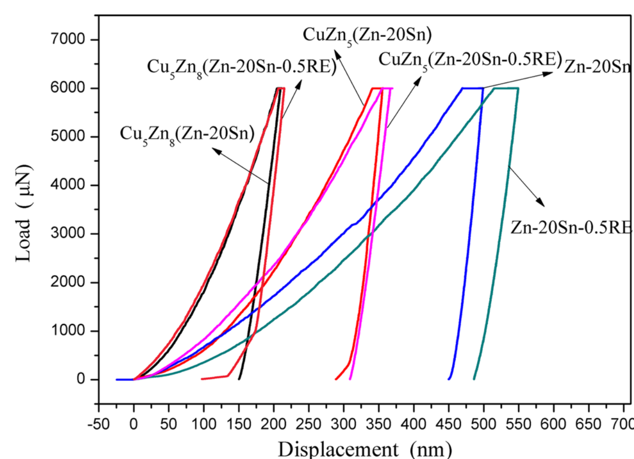

Fig. 6. Load–displacement curves of each phase at the interface.

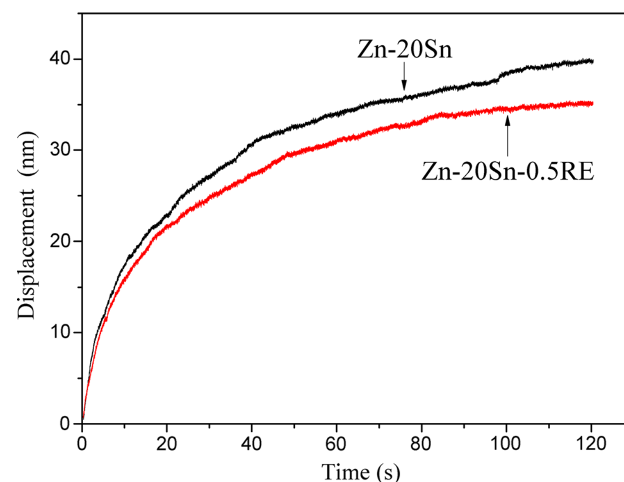

Fig. 7. Creep displacement–creep time curves for solders.

The creep displacement–creep time curves of the solders at maximum load are shown in Fig. 7. The curves can be divided into two stages: the initial stage and the large displacement stages. In the initial stage, the creep displacement increased rapidly, and then slowly increased with time. At large displacement stage, the creep displacement and creep time exhibit an approximate linear relationship. When the maximum load is maintained, the Zn-20Sn-0.5RE solder has a smaller creep displacement than that of Zn-20Sn solder, and its creep resistance is better. After adding 0.5 wt.% RE, some of REs segregate in the surface or at the solid–liquid interface, which reduces the interfacial tension. Some of REs exist as RE-Zn compounds.[8] Stable compounds are distributed in the slip surface, which hinders dislocation movement and improves the solder creep property.

The elastic modulus, hardness and other properties of each phase are shown in Table II. With the transition from solder matrix to interfacial compound, the hardness increases gradually. The

Table II. Data of nano-indentation of solder joints for each phase

Name of the phase	Elastic modulus *E* (GPa)	Hardness *H* (GPa)	*E/H*
Zn-20Sn	65.01 ± 8.84	1.00 ± 0.34	65.0
$CuZn_5$(Zn-20Sn)	71.10 ± 10.96	2.16 ± 0.36	32.9
Cu_5Zn_8(Zn-20Sn)	107.14 ± 2.43	5.45 ± 0.31	19.7
Zn-20Sn-0.5RE	42.28 ± 1.26	0.83 ± 0.10	50.9
$CuZn_5$(Zn-20Sn-0.5RE)	62.26 ± 3.52	1.89 ± 0.10	32.9
Cu_5Zn_8(Zn-20Sn-0.5RE)	117.09 ± 2.14	5.18 ± 0.33	22.6

elastic modulus and indentation hardness of solder is the smallest, followed by ε-$CuZn_5$, and the γ-Cu_5Zn_8 is the largest. The γ-Cu_5Zn_8 layer has large thickness and high hardness, which becomes a brittle phase in the solder joint.

With an increase in E/H, the relative elastic recovery becomes less, hence resulting in a greater degree of plastic deformation.[19] Based on this concept, the E/H values of these phase of the interface were calculated and are listed in Table II. The ability for plasticity of these phase in decreasing order was: Zn-20Sn, Zn-20Sn-0.5RE, $CuZn_5$, Cu_5Zn_8.

The elastic modulus of the IMC $CuZn_5$ (Zn-20Sn) is 9% greater than that of the Zn-20Sn solder. The elastic modulus of the Cu_5Zn_8 (Zn-20Sn) is 64% greater than that of the Zn-20Sn solder. The elastic modulus on both sides of the $CuZn_5$/Cu_5Zn_8 interface has changed abruptly, and has become a weak area of solder joint. From the micro zone mechanical properties, it can be explained that the fracture location of the soldered joints of the Zn-20Sn/Cu is at the $CuZn_5$/Cu_5Zn_8 interface.[2]

CONCLUSIONS

1. The addition of RE has almost no effect on the wetting time at temperature of 410–440°C. The corrosion resistance of the Zn-20Sn-0.5RE solder is improved.
2. RE addition increases thickness of the ε-$CuZn_5$ and γ-Cu_5Zn_8 layer at the soldering interface, promotes bamboo-shoot-like growth of the ε-$CuZn_5$, increases the roughness of the ε-$CuZn_5$ layer at the interface, and improves the shear strength of the soldered joints.
3. After soldering, the creep resistance of the Zn-20Sn-0.5RE solder is improved. With the transition from solder matrix to interfacial compound, the indentation hardness and elastic modulus increased gradually. The elastic modulus on both sides of the $CuZn_5$/Cu_5Zn_8 interface has changed abruptly, and becomes a weak area of soldered joint.

ACKNOWLEDGMENTS

This work was supported by the scientific and technological project in Fujian Province (2015H0008).

REFERENCES

1. S. Menon, E. George, M. Osterman, and M. Pecht, *J. Mater. Sci. Mater. Electron.* 26, 4021 (2015).
2. J.E. Lee, K.S. Kim, K. Suganuma, J. Takenaka, and K. Hagio, *Mater. Trans.* 46, 2413 (2005).
3. S. Kim, K.S. Kim, K. Suganuma, and G. Izuta, *J. Electron. Mater.* 38, 873 (2009).
4. K. Suganuma, S.J. Kim, and K.S. Kim, *JOM* 61, 64 (2009).
5. W.L.R. Santos, C. Brito, J.M.V. Quaresma, J.E. Spinelli, and A. Garcia, *Mater. Sci. Eng., B* 182, 29 (2014).
6. C.W. Liu and K.L. Lin, *J. Electron. Mater.* 43, 4502 (2014).
7. C.M.T. Law, C.M.L. Wu, D.Q. Yu, L. Wang, and J.K.L. Lai, *J. Electron. Mater.* 35, 89 (2006).
8. J. Tian, P. Dai, and X. Li, *J. Mater. Sci. Mater. Electron.* 28, 17185 (2017).
9. D.Q. Yu and L. Wang, *J. Alloys Compd.* 458, 542 (2008).
10. M.K. Choi, C.Y. Lee, C.J. Shur, and J.P. Jung, *J. Electron. Manuf.* 8, 235 (1998).
11. F. Rosalbino, E. Angelini, D. Macciò, A. Saccone, and S. Delfino, *Electrochim. Acta* 52, 7107 (2007).
12. D. Ma, W.D. Wang, and S.K. Lahiri, *J. Appl. Phys.* 91, 3312 (2002).
13. J.K. Shang and D. Yao, *J. Electron. Packag.* 118, 170 (1996).
14. S. Kim, K.S. Kim, S.S. Kim, and K. Suganuma, *J. Electron. Mater.* 38, 266 (2009).
15. B. Lao, S. Gao, and Q. Zhang, *Acta Phys. Chim. Sin.* 17, 453 (2001).
16. X. Deng, N. Chawla, K.K. Chawla, and M. Koopman, *Acta Mater.* 52, 4291 (2004).
17. G.Y. Jang, J.W. Lee, and J.G. Duh, *J. Electron. Mater.* 33, 1103 (2004).
18. A.R. Geranmayeh and R. Mahmudi, *J. Electron. Mater.* 34, 1002 (2005).
19. J.M. Song, M.J. Lin, K.H. Hsieh, T.Y. Pai, Y.S. Lai, and Y.T. Chiu, *J. Electron. Mater.* 42, 2813 (2013).